

Enhancing Ultra High Resolution Remote Sensing Imagery Analysis with ImageRAG

Zilun Zhang [†], Haozhan Shen [†], Tiancheng Zhao, Yuhao Wang,
Bin Chen, Yuxiang Cai, Yongheng Shang, Jianwei Yin

arXiv:2411.07688v1 [cs.CV] 12 Nov 2024

Abstract—Ultra High Resolution (UHR) remote sensing imagery (RSI) (e.g. $100,000 \times 100,000$ pixels or more) poses a significant challenge for current Remote Sensing Multimodal Large Language Models (RSMLLMs). If choose to resize the UHR image to standard input image size, the extensive spatial and contextual information that UHR images contain will be neglected. Otherwise, the original size of these images often exceeds the token limits of standard RSMLLMs, making it difficult to process the entire image and capture long-range dependencies to answer the query based on the abundant visual context. In this paper, we introduce ImageRAG for RS, a training-free framework to address the complexities of analyzing UHR remote sensing imagery. By transforming UHR remote sensing image analysis task to image’s long context selection task, we design an innovative image contextual retrieval mechanism based on the Retrieval-Augmented Generation (RAG) technique, denoted as ImageRAG. ImageRAG’s core innovation lies in its ability to selectively retrieve and focus on the most relevant portions of the UHR image as visual contexts that pertain to a given query. Fast path and slow path are proposed in this framework to handle this task efficiently and effectively. ImageRAG allows RSMLLMs to manage extensive context and spatial information from UHR RSI, ensuring the analysis is both accurate and efficient.

I. INTRODUCTION

In the field of remote sensing (RS), ultra-high-resolution (UHR) images often cover vast areas, encompassing diverse landscapes and a wide range of geospatial features. For deep learning applications such as semantic segmentation, object detection, and change detection, processing these large-scale images directly poses significant challenges. The high spatial resolution results in massive image sizes (e.g. $100,000 \times 100,000$ pixels), making it difficult to directly train neural networks with such images due to the limitation in GPU memory. Additionally, the variability in scale, class distribution, and object sizes within these large images can lead to suboptimal performance if not handled properly. To address these, a common preprocessing step is to cut the original UHR images into smaller patches (e.g. 224×224 or 512×512) [1] [2] that can fit in regular deep learning workflows.

Multimodal Large Language Models (MLLMs, in this paper we specifically refer to Vision-Language Models using LLM as base model) have demonstrated remarkable potential in RS tasks, including image captioning [3], visual grounding [4],

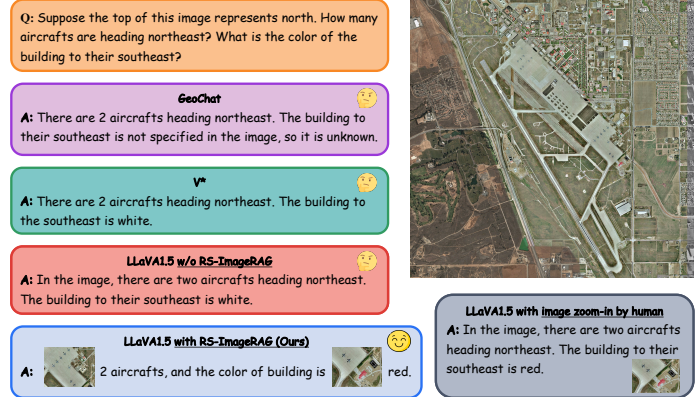


Fig. 1. An example of a challenging question that requires analyzing small targets in a high-resolution image. Models such as GeoChat, LLaVA1.5, and V^* failed to answer. LLaVA1.5 with ImageRAG can answer correctly.

relation reasoning [5], object detection [6], and visual question answering (VQA) [7]. However, the input image resolutions for these Remote Sensing Multimodal Large Language Models (RSMLLMs) are often limited and relatively small compared with the original satellite image. For example, models like LLaVA 1.5 [8] and H2RSVLM [7] utilize image inputs of 336×336 pixels, while Geochat [3] and SkysenseGPT [5] process images at 504×504 pixels. Vision-language models (VLMs) specifically trained for RS, such as GeoRSCLIP [9] and RemoteCLIP [10], work with even smaller inputs, typically at 224×224 pixels.

In Figure 1, we illustrate how current MLLMs struggle to answer a challenging question that requires identifying small objects in a high-resolution (2086×2086) image. The model’s limitations in handling fine details and distinguishing small features become evident, leading to inaccurate responses when tasked with analyzing such intricate visual information (the model can answer correctly when the zoom-in image is provided). We identify four types of approaches for applying MLLMs to UHR RSI, each with its own set of limitations.

The first approach involves resizing UHR images to a smaller size in order to be compatible with current MLLMs. However, this significantly reduces the visibility of small objects in the images, making them challenging to detect, even for humans. For instance, H2RSVLM [7] claims its difficulty in handling small objects, likely due to limitations in input image resolution of 336×336 . The second approach divides UHR images into smaller patches that can be sequentially processed by MLLMs. While this allows for compatibility with existing

[†]: Equal Contribution

Zilun Zhang, Haozhan Shen, Yuhao Wang, Bin Chen, Yuxiang Cai, Yongheng Shang, and Jianwei Yin are with the College of Computer Science and Technology, Zhejiang University, Hangzhou, China; Tiancheng Zhao is with the Binjiang Research Institute of Zhejiang University (e-mail: zilun.zhang@zju.edu.cn; tianchez@zju-bj.com).

model architectures, it results in the loss of global and relative information and relationships present in the original large-scale image, as only portions of the image are considered at a time. The third approach references techniques from general LLMs for managing long context, such as Positional Interpolation [11] and LongROPE [12]. Or adopting architecture from video MLLMs like LongVILA [13], which can extend the context window effectively. This approach could potentially enable the integration of entire UHR images while maintaining global information. However, it would necessitate retraining the models from scratch. The fourth approach employs guided visual search methods that focus on relevant patches, such as V^* [14], or hybrid architectures like LongLLAva [15], which enable the processing of very large input images, and not neglect the small targets. Similar to the drawbacks of the third approach, this method also requires retraining the model and demands task-specific annotations, adding to the complexity and effort needed for implementation.

Three crucial aspects for MLLMs to effectively handle UHR RSI are: (1) managing small targets, ensuring that the model can accurately aware and analyze fine details within images; (2) processing the UHR image in a way that integrates with MLLMs without significantly increasing the number of image tokens, which would lead to high computational costs; and (3) achieving these goals while minimizing the need for additional training or specialized annotation.

To address these problems, we contribute the **ImageRAG** framework for RSMLLMs, which offers several key advantages. First, it retrieves and emphasizes relevant visual context from the UHR image based on the text query, allowing the MLLM to focus on **important details, even tiny ones**. Second, it integrates various **external knowledge sources** to guide the model, enhancing the understanding of the query and the UHR RSI. Lastly, ImageRAG is **training-free**, and requires no additional annotations, making it a practical solution for efficiently handling UHR RSI. **ImageRAG is initially designed for RS, but it is suitable for general tasks and other specific domains, as long as building modules with corresponding data.**

II. THE IMAGERAG FRAMEWORK

As shown in Figure 2 (down), ordinary Retrieval-Augmented Generation (RAG) boosts the capabilities of LLMs by retrieving and referencing relevant document chunks from external knowledge database through the semantic similarity [16] [17]. The process involves two main stages: Retrieval and Generation. In this way, RAG effectively reduces the problem of generating factually incorrect or out-of-date content [18].

A challenge in applying RAG to UHR RSI is how to extend RAG to visual modality. It requires VLMs to associate text and visual embeddings, which may face difficulties in aligning visual concepts in satellite views with corresponding text descriptions. Besides, consider image patches as contexts could result in no visual contexts be found to aid generation. We will expand this and provide a solution in section II-A4.

Our ImageRAG framework for RSMLLM references the idea of RAG, but focusing on retrieving **visual contexts** as

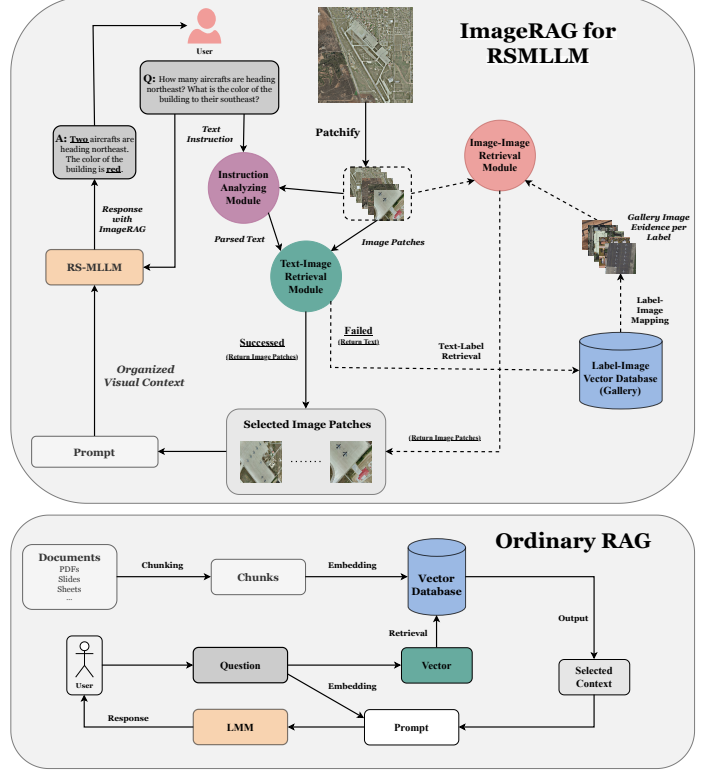


Fig. 2. The ImageRAG Framework (up) and Ordinary RAG (down). **Dashed lines** represent the slow path of ImageRAG, and the **solid lines** represents the fast path. Detail introduction on ImageRAG can be found in section II

evidences for the text query. As shown in Figure 2 (up), ImageRAG also contains two stages, **Retrieval Stage** and **Generation Stage**. We denote a given image as I_i and corresponding text query (instruction) as T_i . The ImageRAG framework aims to **retrieve a set of relevant visual contexts** V_i to augment input and **generate response** R_i . There are two modes for ImageRAG to work, **fast path** and **slow path**.

A. Retrieval Stage

Given an Image I_i , a text query T_i , a **Patch Division Approach** F , an **Instruction Analyzing Module** G , a **Text-Image Retrieval Module** M_{ti} (including image encoder f_{img} , text encoder f_{text} , select function H_{fast} with threshold ϵ), a **Label-Image Vector Database** D with threshold δ , and an **Image-Image Retrieval Module** M_{ii} (including image encoder f_{img} , text encoder f_{text} , select function H_{slow} with threshold ϵ). The visual context V_i can be selected by:

$$V_i = \begin{cases} M_{ti}(I_i, T_i | (F, G, f_{img}, f_{text}, H_{fast})) & \text{for fast path} \\ M_{ii}(I_i, T_i, D | (F, G, f_{img}, f_{text}, H_{slow})) & \text{for slow path} \end{cases}$$

1) Image Patch Division Approach: There are several image patchification approaches. For instance, ViT [19] divides image into fixed-size, non-overlapping grids with dimensions such as 32×32 and 14×14 pixels. The Swin Transformer [20] uses a hierarchical architecture to partition the image at multiple scales, employing shifted windows to capture more diverse contextual information. DetailCLIP [21] introduced the

”Complete Cover” method, which aims to partition the image that patches can cover objects of any scale. The patchification process with patch division approach F can be formulated as:

$$P_i = F(I_i) = \{p_i^j\}_{j=1}^m \quad (1)$$

Where P_i denotes a set of image patches for image I_i .

2) *Instruction Analyzing Module*: The Instruction Analyzing Module G takes vanilla text instruction T_i and outputs a set of key phrases Q_i . The whole process is entirely based on the input text instruction, but for the extendibility of this framework, we add the set of image patches to the input. We formulate the instruction analyzing process as follows:

$$Q_i = G(P_i, T_i) = \{t_i^j\}_{j=1}^n \quad (2)$$

3) *Text-Image Retrieval Module: Relevant visual contexts*
 V_i (a subset of P_i) can be identified with a Text-Image Retrieval Module M_{ti} . This module ensures that the image regions most relevant to the textual contents are selected, enhancing the model’s ability to focus on meaningful image areas for the given query. n key phrases and m image patches will be encoded to text and image embeddings (d-dimension vectors) through a text encoder f_{text} and an image encoder f_{img} , respectively. The similarity matrix between n text embeddings and m image embeddings in this module is denoted as S_{fast} ($S \in \mathbb{R}^{n \times m}$) by calculate the similarities between the embeddings of parsed text key phrases Q_i and the embeddings of image patches P_i .

$$S_{fast} = f_{text}(Q_i) @ f_{img}(P_i).T \quad (3)$$

where @ represents matrix multiplication and T for transpose.

Visual context V_i will be selected based on similarity matrix S_{fast} and similarity threshold ϵ using a selection function H_{fast} .

$$V_i = H_{fast}(P_i, S_{fast}, \epsilon) = \{v_i^j\}_{j=1}^k \quad (4)$$

where k means k patches satisfied the condition and selected as visual context. If $k > 0$, the selected visual context k will send to the RSMLLM directly, which we call **”fast path”**.

4) *Label-Image Vector Database (Gallery)*: If $k = 0$, a more complicate **”slow path”** will be proceed. First, we introduce the Label-Image Vector Database D , which stores million-scale labeled RSI with the key-value pairs as follows: the key is the **text embedding of the class name**, generated using the text encoder f_{text} , and the value is the **mean of the image embedding** obtained using the image encoder f_{image} with the set of images associated with that class.

Given a set of query key phrases $Q_i = \{t_i^j\}_{j=1}^n$, D retrieves the corresponding labels $L_i = \{l_i^p\}$ whose text embeddings have high semantic similarity (i.e. greater than certain threshold δ) with the query embeddings $f_{text}(Q_i)$. Formally, the retrieval process can be expressed as:

$$L_i = \{l_i^p\} = D(f_{text}(Q_i), \delta) \quad (5)$$

where l_i^p represents a label in the database that related to query Q_i , and δ is a similarity threshold. The mean image embeddings associated with the retrieved labels $L_i = \{l_i^p\}$ are then provided as $E_i = \{e_i^p\}$, which forms the set of relevant visual concepts within D for the given queries Q_i .

The motivation behind this step is to address the potential limitations of the Text-Image Retrieval Module M_{ti} , which may not fully understand the visual concept of certain phrases in the domain of remote sensing since M_{ti} could utilize a general VLM rather than RS-specialized one. For instance, the appearance of an aircraft can vary significantly depending on the perspective, such as a main view versus an satellite view. **Fast path failure indicates that no visual concept has been found for the key phrases with high confidence**. However, it is unlikely that a text query would target a ”void” concept since they are proposed by user. A plausible explanation is that Text-Image Retrieval Module M_{ti} utilizes VLM that is trained on general image-text pairs, making VLM is difficult to associate visual concepts in the RS domain with the textual descriptions. To address this, the **slow path leverages the text embeddings of the phrases and labels as anchors and retrieves image embeddings from the RS domain within the database for phrase concepts**. These retrieved image embeddings serve as visual evidence and can be used for image-to-image search later, thereby enhancing the model’s understanding of domain-specific visual concepts.

5) *Image-Image Retrieval Module*: When visual evidence $E_i = \{e_i^p\}$ for each label are obtained, we can calculate the similarity matrix of patches P_i and visual evidence E_i .

$$S_{slow} = E_i @ f_{img}(P_i).T \quad (6)$$

Visual context V_i for **slow path** will be selected based on similarity matrix S_{slow} and similarity threshold ϵ using the selection function H_{slow} .

$$V_i = H_{slow}(P_i, S_{slow}, \epsilon) = \{v_i^j\}_{j=1}^k \quad (7)$$

B. Generation Stage

Once visual contexts V_i are selected from P_i , a set of image patches from image I_i , RS-MLLM can use such visual contexts for response generation. Unlike Ordinary RAG, which can directly organize retrieved text content with a prompt and send to a LLM to generate the response, ImageRAG must handle visual context. This means ImageRAG needs to select a MLLM that can utilize the visual contexts as visual cues.

VQA LLM from V^* framework [14] is chosen alone with the specifically designed prompt since it is trained for accepting additional visual information to focus on. The response R_i for given image I_i and text query T_i is calculated by:

$$R_i = \text{VQALLM}(I_i, V_i, T_i | \text{Prompt}) \quad (8)$$

C. Implementation Detail

For the prototype of ImageRAG, we choose Complete Cover [21] from DetailCLIP to be the **Patch Division Approach** F , which brings 166 patches per Image. The **Instruction Analyzing Module** G is implemented by KeyBERT [22] with ngram range up to 4 and a maximal of top-10 phrases per text query. f_{img} and f_{text} are implemented by image encoder and text encoder of CLIP-ViT-L-336px [23]. H_{fast} and H_{slow} select top 10 patches from S_{fast} and S_{slow} , respectively. The **Label-Image Vector Database** D is naively implemented with pickle

and dictionary, which plan to be replaced by HyperDB¹ in the full paper. We currently use data from FMoW [24] to setup the database. We retrained the **VQALLM** following V^* paper with LLaVA-1.5 structure.

III. FLEXIBILITY AND EXTENDABILITY

Section II-C presents a prototype design of the ImageRAG framework, showcasing its foundational architecture. Moreover, ImageRAG is designed with considerable flexibility and extendability, allowing each module to be expanded or upgraded with more advanced versions as needed.

A. Instruction Analyzing Module

More sophisticated approaches can enhance the process of extracting key phrases from the text query compared with KeyBERT. For instance, incorporating the image as an input to this module enables the use of region captioning and object detection models, which can enrich and paraphrase the text query with additional contextual information.

Latitude and longitude information can be estimated using geo-localization models [25] and ground models [26]. The ground and satellite view can be aligned for cross-reference. This inferred location information allows for retrieving nearby information from sources like OpenStreetMap, thereby improving the precision and relevance of the query analysis.

Besides, scene graph for large-size satellite imagery [27] can be included as well to better analyze the important premise of the text query and possible relations within the image patches.

B. Label-Image Vector Database

The text retrieval process, which employs a set of key query phrases Q_i to identify relevant labels L_i , can be enhanced by expanding the definitions or explanations of both the key phrases and labels. The retrieval process can achieve more accurate matching based on these expanded explanations.

The ultimate goal of the D is to retrieve visual concepts within the RS domain based on text input. This retrieval process can be considered as a recommendation system problem, where labels are viewed as users and the visual concepts associated with these labels are seen as items. In this framework, User-User and User-Item recommendation algorithms can be applied, allowing the system to suggest relevant visual concepts (items) based on the given text query (user). This approach enables efficient and contextually accurate retrieval of visual data that aligns closely with the query's intent.

The representation of embeddings for visual concepts of each class can be further refined. This is a well-studied problem in Few-Shot Learning and Long-Tailed Recognition. In our prototype design, the mean image embedding is calculated from all images sharing the same class label, following the approach of ProtoNet [28]. However, more sophisticated representations such as clustering centroids, class centers, inter-class margin and intra-class diversity balancing could be further investigated to enhance visual concept representations. Such improvements could lead to better recall in the retrieval.

Additional data sources, such as MillionAID [29], SatlasPretrain [30], FAIR1M [31], and Satellogic-EarthViewer², can be integrated into D to enrich its scope and diversity. To further reduce noise and improve data quality, image patches cropped with bounding boxes can be added, enhancing the image embeddings by eliminating irrelevant noise.

C. Multimodal Large Language Model with Visual Prompt

The VQA LLM from V^* could be further replaced by training-free models such as ControlMLLM [32], or more powerful models that use bounding boxes as visual prompts like Ferretv2 [17]. These methods could potentially boost the VQA capability of MLLMs with given visual cues.

IV. EVALUATION

We design two types of benchmarks to evaluate ImageRAG in Referring Expression Task: **filtered existing benchmarks for small targets** and a **new benchmark for UHR RSI**.

TABLE I
STATISTICS OF NUMBER OF QUERY FOR FILTERED EXISTING RS VQA BENCHMARKS (TEST SET FOR REFERRING EXPRESSION TASK ONLY)

Dataset	# Unfiltered	# ratio < 0.001	# ratio < 0.0001
FIT-RSFG [5]	11,174	1,175	21
VRSBench [6]	16,159	2,758	48

The advantage of the former is its simplicity to acquire, requiring only filtering of current benchmarks based on the ratio of target area to image area in each query (e.g., ratios below 0.001 or 0.0001). Statistics for obtained benchmarks are shown in Table I. We trained a SkysenseGPT following [5], and test the model in unfiltered and filtered (ratio < 0.001) FIT-RSFG. We observed the mAP in Object Detection task drops from 28.25 to 5.07, and F1 in Relation Reasoning task drops from 79.75 to 69.88. However, the filtered benchmarks do not fully match our intention on handling UHR RSI.

The latter benchmark, on the other hand, is more realistic and involves end-to-end VQA within a UHR RSI, enabling the model to consider complex inter-object relationships and closely reflect real-world scenarios. The drawback of this approach is the substantial annotation effort required. For example, if we choose to merge split images (e.g., 512×512) into a single UHR image from existing datasets, all corresponding annotations would need to be re-labeled to account for shifts in relative relationships between objects. Not mentioned construct the UHR RSI dataset for RET from scratch.

¹<https://github.com/jdagdelen/hyperDB>

²<https://huggingface.co/spaces/satellogic/EarthView-Viewer>

REFERENCES

- [1] G.-S. Xia, X. Bai, J. Ding, Z. Zhu, S. Belongie, J. Luo, M. Datcu, M. Pelillo, and L. Zhang, "Dota: A large-scale dataset for object detection in aerial images," in *The IEEE Conference on Computer Vision and Pattern Recognition (CVPR)*, June 2018.
- [2] S. Waqas Zamir, A. Arora, A. Gupta, S. Khan, G. Sun, F. Shahbaz Khan, F. Zhu, L. Shao, G.-S. Xia, and X. Bai, "isaid: A large-scale dataset for instance segmentation in aerial images," in *Proceedings of the IEEE Conference on Computer Vision and Pattern Recognition Workshops*, 2019, pp. 28–37.
- [3] K. Kuckreja, M. S. Danish, M. Naseer, A. Das, S. Khan, and F. S. Khan, "Geochat: Grounded large vision-language model for remote sensing," *The IEEE/CVF Conference on Computer Vision and Pattern Recognition*, 2024.
- [4] W. Zhang, M. Cai, T. Zhang, Y. Zhuang, and X. Mao, "Earthgpt: A universal multi-modal large language model for multi-sensor image comprehension in remote sensing domain," 2024. [Online]. Available: <https://arxiv.org/abs/2401.16822>
- [5] J. Luo, Z. Pang, Y. Zhang, T. Wang, L. Wang, B. Dang, J. Lao, J. Wang, J. Chen, Y. Tan, and Y. Li, "Skysensegt: A fine-grained instruction tuning dataset and model for remote sensing vision-language understanding," *arXiv preprint arXiv:2406.10100*, 2024.
- [6] X. Li, J. Ding, and M. Elhoseiny, "Vrsbench: A versatile vision-language benchmark dataset for remote sensing image understanding," 2024. [Online]. Available: <https://arxiv.org/abs/2406.12384>
- [7] C. Pang, J. Wu, J. Li, Y. Liu, J. Sun, W. Li, X. Weng, S. Wang, L. Feng, G.-S. Xia, and C. He, "H2rsvlm: Towards helpful and honest remote sensing large vision language model," 2024. [Online]. Available: <https://arxiv.org/abs/2403.20213>
- [8] H. Liu, C. Li, Y. Li, and Y. J. Lee, "Improved baselines with visual instruction tuning," 2023.
- [9] Z. Zhang, T. Zhao, Y. Guo, and J. Yin, "Rs5m and georsclip: A large scale vision-language dataset and a large vision-language model for remote sensing," *IEEE Transactions on Geoscience and Remote Sensing*, pp. 1–1, 2024.
- [10] F. Liu, D. Chen, Z. Guan, X. Zhou, J. Zhu, Q. Ye, L. Fu, and J. Zhou, "Remoteclip: A vision language foundation model for remote sensing," *IEEE Transactions on Geoscience and Remote Sensing*, vol. 62, pp. 1–16, 2024. [Online]. Available: <https://doi.org/10.1109/TGRS.2024.3390838>
- [11] S. Chen, S. Wong, L. Chen, and Y. Tian, "Extending context window of large language models via positional interpolation," 2023. [Online]. Available: <https://arxiv.org/abs/2306.15595>
- [12] Y. Ding, L. L. Zhang, C. Zhang, Y. Xu, N. Shang, J. Xu, F. Yang, and M. Yang, "Longropic: Extending llm context window beyond 2 million tokens," 2024. [Online]. Available: <https://arxiv.org/abs/2402.13753>
- [13] F. Xue, Y. Chen, D. Li, Q. Hu, L. Zhu, X. Li, Y. Fang, H. Tang, S. Yang, Z. Liu, E. He, H. Yin, P. Molchanov, J. Kautz, L. Fan, Y. Zhu, Y. Lu, and S. Han, "Longvila: Scaling long-context visual language models for long videos," 2024. [Online]. Available: <https://arxiv.org/abs/2408.10188>
- [14] P. Wu and S. Xie, "V*: Guided visual search as a core mechanism in multimodal llms," 2023. [Online]. Available: <https://arxiv.org/abs/2312.14135>
- [15] X. Wang, D. Song, S. Chen, C. Zhang, and B. Wang, "Longllava: Scaling multi-modal llms to 1000 images efficiently via a hybrid architecture," 2024. [Online]. Available: <https://arxiv.org/abs/2409.02889>
- [16] X. Zhao, D. Li, Y. Zhong, B. Hu, Y. Chen, B. Hu, and M. Zhang, "Seer: Self-aligned evidence extraction for retrieval-augmented generation," *arXiv preprint arXiv:2410.11315*, 2024.
- [17] H. Zhang, H. You, P. Dufter, B. Zhang, C. Chen, H.-Y. Chen, T.-J. Fu, W. Y. Wang, S.-F. Chang, Z. Gan, and Y. Yang, "Ferret-v2: An improved baseline for referring and grounding with large language models," 2024. [Online]. Available: <https://arxiv.org/abs/2404.07973>
- [18] Y. Gao, Y. Xiong, X. Gao, K. Jia, J. Pan, Y. Bi, Y. Dai, J. Sun, M. Wang, and H. Wang, "Retrieval-augmented generation for large language models: A survey," 2024. [Online]. Available: <https://arxiv.org/abs/2312.10997>
- [19] A. Dosovitskiy, L. Beyer, A. Kolesnikov, D. Weissenborn, X. Zhai, T. Unterthiner, M. Dehghani, M. Minderer, G. Heigold, S. Gelly, J. Uszkoreit, and N. Houlsby, "An image is worth 16x16 words: Transformers for image recognition at scale," 2021. [Online]. Available: <https://arxiv.org/abs/2010.11929>
- [20] Z. Liu, Y. Lin, Y. Cao, H. Hu, Y. Wei, Z. Zhang, S. Lin, and B. Guo, "Swin transformer: Hierarchical vision transformer using shifted windows," 2021. [Online]. Available: <https://arxiv.org/abs/2103.14030>
- [21] Z. Zhang, C. Shen, Y. Shen, H. Xiong, and X. Zhou, "Injecting image details into clip's feature space," 2023. [Online]. Available: <https://arxiv.org/abs/2208.14649>
- [22] M. Grootendorst, "Keybert: Minimal keyword extraction with bert," 2020. [Online]. Available: <https://doi.org/10.5281/zenodo.4461265>
- [23] A. Radford, J. W. Kim, C. Hallacy, A. Ramesh, G. Goh, S. Agarwal, G. Sastry, A. Askell, P. Mishkin, J. Clark, G. Krueger, and I. Sutskever, "Learning transferable visual models from natural language supervision," 2021.
- [24] G. Christie, N. Fendley, J. Wilson, and R. Mukherjee, "Functional map of the world," 2018. [Online]. Available: <https://arxiv.org/abs/1711.07846>
- [25] V. V. Cepeda, G. K. Nayak, and M. Shah, "Geoclip: Clip-inspired alignment between locations and images for effective worldwide geolocation," 2023. [Online]. Available: <https://arxiv.org/abs/2309.16020>
- [26] U. Mall, C. P. Phoo, M. K. Liu, C. Vondrick, B. Hariharan, and K. Bala, "Remote sensing vision-language foundation models without annotations via ground remote alignment," 2023. [Online]. Available: <https://arxiv.org/abs/2312.06960>
- [27] Y. Li, L. Wang, T. Wang, X. Yang, J. Luo, Q. Wang, Y. Deng, W. Wang, X. Sun, H. Li, B. Dang, Y. Zhang, Y. Yu, and J. Yan, "Star: A first-ever dataset and a large-scale benchmark for scene graph generation in large-size satellite imagery," 2024. [Online]. Available: <https://arxiv.org/abs/2406.09410>
- [28] J. Snell, K. Swersky, and R. S. Zemel, "Prototypical networks for few-shot learning," 2017. [Online]. Available: <https://arxiv.org/abs/1703.05175>
- [29] Y. Long, G.-S. Xia, S. Li, W. Yang, M. Y. Yang, X. X. Zhu, L. Zhang, and D. Li, "On creating benchmark dataset for aerial image interpretation: Reviews, guidances and million-aid," *IEEE Journal of Selected Topics in Applied Earth Observations and Remote Sensing*, vol. 14, pp. 4205–4230, 2021.
- [30] F. Bastani, P. Wolters, R. Gupta, J. Ferdinando, and A. Kembhavi, "Satlaspretrain: A large-scale dataset for remote sensing image understanding," 2023. [Online]. Available: <https://arxiv.org/abs/2211.15660>
- [31] X. Sun, P. Wang, Z. Yan, F. Xu, R. Wang, W. Diao, J. Chen, J. Li, Y. Feng, T. Xu, M. Weinmann, S. Hinz, C. Wang, and K. Fu, "Fair1m: A benchmark dataset for fine-grained object recognition in high-resolution remote sensing imagery," 2021. [Online]. Available: <https://arxiv.org/abs/2103.05569>
- [32] M. Wu, X. Cai, J. Ji, J. Li, O. Huang, G. Luo, H. Fei, G. Jiang, X. Sun, and R. Ji, "Controlmllm: Training-free visual prompt learning for multimodal large language models," 2024. [Online]. Available: <https://arxiv.org/abs/2407.21534>